

3-Dimensional Simulations of the Reorganization of a Quark Star's Magnetic Field as Induced by the Meissner Effect

Rachid Ouyed^{1,2}, Brian Niebergal¹, Wolfgang Dobler¹ and Denis Leahy¹

¹*Department of Physics and Astronomy, University of Calgary, 2500 University Drive NW, Calgary, Alberta, T2N 1N4 Canada*

²*Canadian Institute for Theoretical Astrophysics, University of Toronto, Toronto, Ontario, Canada*

ouyed@phas.ucalgary.ca

ABSTRACT

In a previous paper (Ouyed et al. 2004) we presented a new model for soft gamma-ray repeaters (SGR), based on the onset of colour superconductivity in quark stars. In this model, the bursts result from the reorganization of the exterior magnetic field following the formation of vortices that confine the internal magnetic field (the Meissner effect). Here we extend the model by presenting full 3-dimensional simulations of the evolution of the inclined exterior magnetic field immediately following vortex formation. The simulations capture the violent reconnection events in the entangled surface magnetic field as it evolves into a smooth, more stable, configuration which consists of a dipole field aligned with the star's rotation axis. The total magnetic energy dissipated in this process is found to be of the order of 10^{44} erg and, if it is emitted as synchrotron radiation, peaks typically at 280 keV. The intensity decays temporally in a way resembling SGRs and AXPs (anomalous X-ray pulsars), with a tail lasting from a few to a few hundred times the rotation period of the star, depending on the initial inclination between the rotation and dipole axis. One of the obvious consequences of our model's final state (aligned rotator) is the suppression of radio-emission in SGRs and AXPs following their bursting era. We suggest that magnetar-like magnetic field strength alone cannot be responsible for the properties of SGRs and AXPs, while a quark star entering the "Meissner phase" is compatible with the observational facts. We compare our model to observations and highlight our predictions.

Subject headings: gamma rays: bursts — X-rays: stars — stars: magnetic fields — stars: neutron — stars: quark star

1. Introduction

Soft γ -ray repeaters (SGRs) are sources of recurrent, short ($t \sim 0.1$ s), intense ($L \sim 10^3$ – $10^4 L_{\text{Edd}}$) bursts of γ -ray emission with a soft energy spectrum. The normal pattern of SGR activity are in-

tense activity periods which can last weeks or months, separated by quiescent phases lasting years or decades. The five known SGRs are located in our Galaxy or, in the case of SGR 0526-66, in the Large Magellanic Cloud. The two most intense SGR bursts ever recorded were the 5 March 1979 giant flare of SGR 0526-66 (Mazets et al. 1979) and the similar 27 August 1998 giant flare of SGR 1900+14. The peak luminosities of these events ($\sim 10^6$ – $10^7 L_{\text{Edd}}$) exceeded the peak luminosities of “normal” SGR bursts by a factor $> 10^3$. Several SGRs have been found to be X-ray pulsars with an unusually high spin-down rate of $\dot{P}/P \sim 10^{-10} \text{ s}^{-1}$, usually attributed to magnetic braking caused by a super-strong magnetic field $B > 10^{14} \text{ G}$, which leads to the interpretation that SGRs are magnetars (Golenetskij et al. 1979; Duncan & Thompson 1992, Kouveliotou et al. 1998, Kouveliotou et al. 1999). In the magnetar model, the magnetic field is the likely provider of the burst energy. A common scenario assumes that magnetic stresses create a quake in the crust of the neutron star, which then ejects hot plasma Alfvén waves through its rigid magnetosphere (Thompson & Duncan 1995; 1996). The magnetic field of such a star would have grown to magnetar-scale strengths because of strong convection during the collapse of the proto-neutron star core (Duncan & Thompson 1992; Thompson & Duncan 1993).

1.1. Open issues in the magnetar model of SGRs

In the magnetar model of SGRs, which is also that of Anomalous X-ray Pulsars (AXPs), the X-rays are ultimately powered by an internally decaying very strong magnetic field. However there are still a few open questions which in our opinion leave room for new models to be explored:

- Despite numerous attempts, no magnetars have been detected at radio frequencies¹ (Kriss et al. 1985; Coe et al. 1994; Lorimer et al. 1998; Gaensler et al. 2001). It has been suggested that QED processes at high B , such as photon splitting, may preclude the electron/positron cascades necessary to produce radio emission (Baring&Harding 2001), or that pair production ceases above some critical magnetic field (Zhang & Harding 2000). These ideas or alternatives remain to be confirmed and are still debatable.
- One might expect high- B radio pulsars to be more X-ray bright than low- B sources, and to possibly exhibit AXP-like burst emission. However X-ray observations of 5 high- B radio pulsars reveal luminosities much smaller (by a few orders of magnitudes) than those of AXPs (Pivovaroff et al. 2000; Gonzalez & Safi-Harb 2003; McLaughlin et al. 2003; Gonzalez et al. 2004; Kaspi & McLaughlin 2005). This has lead to suggestions that high- B radio pulsars may one day emit transient AXP-like emission, and conversely that the transient AXPs might eventually exhibit radio pulsations (Kaspi & McLaughlin 2005) – a notion yet to be confirmed.
- Hints of massive (> 30 – $40 M_{\odot}$) progenitors associated with AXPs and SGRs by recent ob-

¹Detecting radio pulsations may be difficult, given the small polar caps implied by the long spin periods.

servations (Gaensler et al. 2005) has led to the suggestion that pulsars and SGRs differ in their progenitor masses. It is also suggested that massive progenitors could lead to neutron stars with millisecond periods (Heger et al. 2004) which would comply with the magnetar model for SGRs (Duncan & Thompson 1992). This, however, leaves open the question of why high- B pulsars, formed from less massive progenitors (presumably with periods > 15 ms), possess magnetar-like field strengths.

- All SGRs and AXPs known to date have spin periods between 6 and 12 seconds (Kaspi 2004). This clustering in period remains to be explained by the magnetar model.

Here we explore an alternative model first presented by Ouyed et al. (2004) where one assumes that AXPs and SGRs are quark stars, rather than magnetars. While quark stars have yet to be found in nature, formation scenarios have been suggested in the literature (see Sect. 8.4 in Ouyed et al. 2004 and references therein). The qualitative idea is that the core of a neutron star reaches deconfinement densities, eventually leading to the conversion of the entire star to a quark star. In principle, the transition from hadronic matter into quark matter in the core of a neutron star can happen immediately during or after the supernova explosion, but also much later than that. Such a transition could occur in a smooth stable manner (e.g. Bombaci & Datta 2000 and references therein) or in an explosive manner termed the “Quark-Nova” (Ouyed et al. 2002; Keränen, Ouyed, & Jaikumar 2005). In these formation scenarios, if the quark star is born shortly after the supernova, the emitted energy/radiation would be absorbed by the still expanding supernova ejecta, and there would be no detectable signature of the transition. The hadron-quark transition may also happen much later than the supernova explosion and could be induced, for example, by accretion if the neutron star is a member of a binary, or via spin-down in the case of isolated neutron stars. The new idea of this model, first presented in Ouyed et al. (2004), is that the quark star enters a superconductive phase, and subsequently experiences a “Meissner phase” that triggers the reorganization of the star’s magnetic field. Before going into more details we first describe properties of quark matter and the concept of color superconductivity.

1.2. Superconductivity and Meissner effect in quark stars

The discovery of asymptotic freedom, leading to the formulation of quantum chromodynamics (QCD) as the theory of strong interactions, was soon followed by the suggestion that matter at sufficiently high densities consists of a deconfined phase of quarks (Collins & Perry 1975). Only shortly afterwards it was pointed out (Barrois 1977) that the true ground state of cold dense quark matter exhibits color superconductivity (CSC), characterized by diquark condensation with an estimated energy gap $\Delta \simeq 1$ MeV between the highest occupied and the unperturbed quark state at the Fermi surface. Since this magnitude of the gap is rather small for phenomenological applications, CSC subsequently received little attention. The situation changed when investigations (Alford, Rajagopal, & Wilczek 1998; Rapp et al. 1998), using nonperturbative forces (e.g.,

instanton-induced), showed that the gap can be substantially larger, $\Delta \simeq 100$ MeV for moderate quark chemical potentials, $\mu_q \simeq 350$ MeV. Similarly large values are obtained from estimates based on perturbative calculations at asymptotically high densities (Pisarski & Rischke 1999; Son 1999). Thus, from the practical point of view, the existence of color superconductivity in compact stars has (re-)emerged as an exciting possibility.

The detailed properties of CSC matter relevant to astrophysical applications depend on the interplay of the quark chemical potential, the q - q interaction strength, and the bare masses of the (light) quarks u , d and s . In particular, for μ_q below the (constituent) strange quark mass, only u and d quarks are subject to Cooper pairing. The corresponding phase is known as 2-flavor CSC (2SC). In the idealized case where the quark chemical potential is much larger than the strange quark mass (m_s), the latter becomes negligible and all three flavors exhibit likewise pairing. The preferred symmetry (breaking) pattern in this phase corresponds to the so-called color-flavor locking (CFL; Alford, Rajagopal, & Wilczek 1999), since the underlying diquark condensate is invariant only under simultaneous color and flavor transformations. In the present work, we will focus on the CFL phase (for a recent review and a more exhaustive list of references, cf. Schäfer 2003). Associated with CSC is the critical temperature, $k_B T_c \sim 0.5 \Delta$, above which pairing is washed out.

One of the most interesting properties of an ordinary superconductor is the Meissner effect, i.e., the expulsion of magnetic flux from the superconductor (Meissner & Ochsenfeld 1933). In the CFL phase, the gauge bosons connected with the broken generators obtain masses, which indicates the Meissner screening effect (Rischke 2000a,b). This is the heart of our model which we describe next.

1.3. Our model

Assume a quark star is born with a temperature $T > T_c$ and enters the CFL phase as it cools by neutrino emission (Keränen, Ouyed & Jaikumar 2005). The CFL front quickly expands to the entire star followed by the formation of rotationally induced vortices, analogous to rotating superfluid ^3He (the vortex lines are parallel to the rotation axis; Tilley&Tilley 1990). Via the Meissner effect, the magnetic field is partially screened from the regions outside the vortex cores. The system now consists of alternating regions of superconducting material with a screened magnetic field, and the vortices where most of the magnetic field resides. As discussed in Ouyed et al. (2004), this has interesting consequences on how the surface magnetic field can adjust to the interior field which is pinned to the vortices. Figure 1 shows the starting point for this reorganization of the magnetic field, just after the Meissner effect has fully aligned the magnetic flux inside the star with the rotation axis. Within a transition region, the magnetic field switches from the vertical interior field to that of an inclined dipole outside. A conservative assumption (from the energetics point of view) is that the field in the transition region is a potential field (minimum-energy configuration).

In order to capture the complex non-linear dynamics of the system we need the help of 3-D

simulations. These simulations will allow us to follow the evolution and re-organization of the magnetic field induced by the vortices.

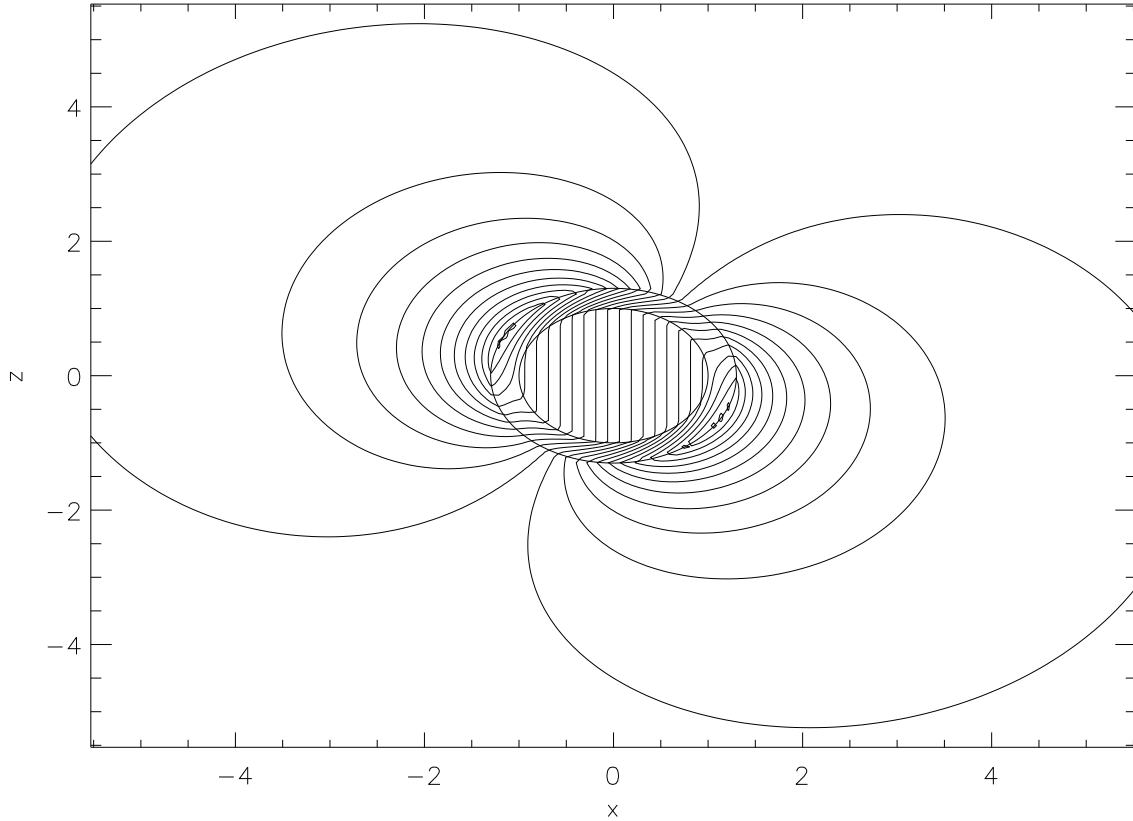


Fig. 1.— “Mock magnetic field lines” at $t = 0$ in the xz -plane. The rotation axis is in the z direction inclined by an angle θ with respect to the dipole axis. Initial state after the stars interior converts to the CFL phase thus causing the magnetic field to be confined inside the vortices. The inner circle represents the surface of the star, and between that and the outer circle is the region where surface currents cause the outer dipole field to adjust to the vortex-aligned inner field. Shown are isolines of the vector potential component A_y , which for our setup trace most features of magnetic field lines.

The paper is presented as follows: In § 2 we describe and analyze the basic setup of our simulations. We calculate the synchrotron light curves that result from the simulations wherein we find remarkable similarities to SGR light curves. Mechanisms for the observed subsequent bursts and the quiescent phase in SGRs are then briefly discussed in terms of our model in § 3. In § 4 we discuss the model predictions and how it can account, at least in its current stage, for the points listed in § 1.1. Here we suggest a list of observations that could test our model. We conclude in § 5.

2. Simulations

Two fundamental parameters of our model are the inclination angle θ of the external dipole field relative to the rotation axis, and β , the initial ratio of gas to magnetic pressure at the surface. The simulations start with the interior magnetic field confined in vertical vortices for $r < R_{\text{QS}}$, but with a still unperturbed inclined dipole field for $r > 1.3 R_{\text{QS}}$. The transition region $R_{\text{QS}} < r < 1.3 R_{\text{QS}}$ is filled by a potential field and is bounded by two current layers (see Fig. 1). The whole configuration was chosen by minimizing the total magnetic energy (see Appendix B).

We solve the following set of non-ideal magnetohydrodynamical (MHD) equations, using the PENCIL-CODE (see *e.g.* Dobler et al. 2006)².

$$\frac{D \ln \varrho}{Dt} = -\nabla \cdot \vec{u} \quad (1)$$

$$\begin{aligned} \frac{D \vec{u}}{Dt} = & -c_s^2 \nabla \left(\frac{s}{c_p} + \ln \varrho \right) - \nabla \Phi_{\text{grav}} + \frac{\vec{j} \times \vec{B}}{\varrho} \\ & + \nu \left(\nabla^2 \vec{u} + \frac{1}{3} \nabla \nabla \cdot \vec{u} + 2\mathbf{S} \cdot \nabla \ln \varrho \right) \end{aligned} \quad (2)$$

$$\frac{\partial \vec{A}}{\partial t} = \vec{u} \times \vec{B} - \eta \mu_0 \vec{j} \quad (3)$$

$$\varrho T \frac{Ds}{Dt} = \nabla \cdot (K \nabla T) + \eta \mu_0 \vec{j}^2 + 2\varrho \nu \mathbf{S}^2. \quad (4)$$

Here ϱ , \vec{u} , \vec{A} , and s are density, velocity, magnetic vector potential, and specific entropy, respectively. Parameters and functions kept constant were c_p , Φ_{grav} , ν and η corresponding to specific heat, gravity potential, kinematic viscosity and magnetic diffusivity respectively. The remaining variables c_s , \vec{j} , \vec{B} , \mathbf{S} and T represent the sound speed, electric current density, magnetic flux density, traceless rate-of-strain tensor, and temperature, respectively.

The length scale is in units of the radius of the quark star, R_{QS} , density in units of the star's surface density, ρ_0 , and time is in units of the spin-period, $1/\Omega$. This implies that velocities are in units of $R_{\text{QS}}\Omega$, while the magnetic field is in units of $\sqrt{\rho_0}R_{\text{QS}}\Omega$. The strength of the (dipole) magnetic field at the surface can be estimated for a given β_0 as, $B_0^2 = 8\pi P_0/\beta_0$, where P_0 is the pressure at the surface of the star. Using hydrostatic balance and the perfect gas law this becomes,

$$\begin{aligned} B_0 \sim & \frac{5 \times 10^{13} \text{ G}}{\sqrt{\beta_0}} \times \\ & \left(\frac{\rho_0}{10^6 \text{ g/cm}^3} \right)^{1/2} \left(\frac{10 \text{ km}}{R_{\text{QS}}} \right)^{1/2} \left(\frac{M_{\text{QS}}}{M_{\odot}} \right)^{1/2}. \end{aligned} \quad (5)$$

In the equation above, ρ_0 is the average density of the gas close to the surface of the star. This corona is supplied by fall-back material following the formation of the QS (Keränen, Ouyed, &

²<http://www.nordita.dk/software/pencil-code> – The Pencil Code is a high-order finite-difference code for solving the compressible hydromagnetic equations.

Jaikumar 2005) similar to what has been suggested in the supernova case (Chevalier 1989). The density of the fallback matter, representative of the crust material of the parent neutron star, is estimated to be of the order of 10^6 g cm $^{-3}$.

Note that our MHD equations (1)–(4) are non-relativistic. While near the surface of the quark star some aspects of the physics will be considerably changed by relativistic effects, we expect that the overall dynamics will not be vastly different in a more realistic calculation.

All figures shown here are for resolution 128^3 . We have run simulations at higher resolution, but found that they differ little as far as energetics and evolution are concerned.

2.1. Evolution and reorganization of the surface magnetic field

Figures 2–3 show the evolution of the exterior magnetic field as it adjusts to the vortex-confined field³.

The complicated structure of the surface magnetic field is clearly seen in the animations driven by the frequent magnetic reconnections as the surface field tries to align itself with the interior one (rotation axis). These random reconnection events would bear many similarities to the initial events (*i.e.* those near $t = 0$), but we expect them to be less energetic as the magnetic field slowly decays and weakens. Eventually, the magnetic field evolves into a stable configuration (see Fig. 2) after which the star enters a quiescent phase.

The restructuring of the field in the transition region leads to an approximately spherical Alfvén wave traveling outwards (see Fig. 2 for $t = 1$) and is more prominent in simulations with a stronger magnetic field (*i.e.* smaller β). As the wave travels outwards it amplifies the magnetic field in certain regions causing them to undergo reconnection, which both distorts the wave and eventually damps it out. Furthermore, the regions that underwent reconnection appear to show slow oscillatory motions between the reconnection site and the surrounding gas (“breathing”). This can be seen in the series of diminishing pulses in Fig. 6 and the frequency of the pulses remains nearly constant (see Fig. 7). We note that these pulses appear more prominently in simulations with lower β and do not arise in simulations with $\beta > 1$.

2.2. Energetics and emission

The magnetic energy released in the organization is shown in Fig. 6 and can be cast into a simple equation,

$$E_M \sim 10^{44} \text{ erg} \left(\frac{\alpha}{0.5} \right)^2 \left(\frac{B}{5 \times 10^{13} \text{ G}} \right)^2 \left(\frac{R_{\text{QS}}}{10 \text{ km}} \right)^3, \quad (6)$$

³See the “Animations” link at <http://www.capca.ucalgary.ca> for movies of the simulations.

where α is the fraction of the surface magnetic field that decayed via reconnection events. From Fig. 4 we can infer the decay in magnetic energy to be roughly $\alpha = 0.4 - 0.6$.

Furthermore, if we assume the electrons to be co-rotating ($\gamma_e \sim 1$), then the intensity emitted by synchrotron processes from the simulated region goes as $I_s \propto n_e B^2$. Also, assuming peak emission is at $\nu_p = 0.29\nu_c$, where ν_c is the critical frequency (see Sects. 6.2 and 6.4 in Rybicki & Lightman 1979), we find this emission to be in the X-ray band,

$$h\nu_p \sim 335 \text{ keV} \left(\frac{B}{5 \times 10^{13} \text{ G}} \right) \times \left[1 - 0.29 \left(\frac{M_{\text{QS}}}{M_{\odot}} \right) \left(\frac{10 \text{ km}}{R_{\text{QS}}} \right) \right]^{1/2}, \quad (7)$$

where gravitational redshift is included in the last term. This intensity decays temporally in a way closely resembling SGR bursts (see Fig. 6). The decay profiles of our simulated bursts depend on the initial plasma β at the surface of the star and on the dipole inclination θ . Varying these parameters in our model allows us to fit the exponential decay shape and duration of observed bursts.

2.3. Periodicity in emission

The oscillations shown in Fig. 7, can be interpreted as magnetic “breathing” modes. In this situation, regions where magnetic reconnection occurs cause a disparity in the magnetic pressure between neighbouring regions. This low pressure region will draw plasma in from the surrounding regions causing either more reconnection or enhanced density where, in either case, there will be oscillations in the emission (*i.e.* $n_e B^2$).

Furthermore, since our simulation is performed in the co-rotating frame, our model is too simplistic to reproduce a spin-modulated pattern (e.g. the 8.0 s period observed in the March 5 event) superimposed on a smooth exponential decay in the light curves. However, as can be seen in Figs. 2–3, there are hotter regions with more magnetic reconnection events than others, and so spin modulation should occur naturally. We note that a few of these hot spots appear simultaneously at random locations, implying spin-modulation may consist of even smaller sub-pulses, therefore producing many harmonics in the light curve. In other words, if our model is a correct representation of SGRs, observations could constrain the number of hot spots.

3. Subsequent bursts and quiescent phase

We note that since the CFL phase transition occurs only once in a given star, there is only one giant burst in our model. However, if we assume some form of heating, then it is possible that the quark star can revert to a non-CFL state wherein superconductivity is lost, and the interior

magnetic field lines are no longer constrained to the vortices. Then presumably the dynamics that initially caused the magnetic dipole axis to misalign with the rotation axis, we speculate, should once again ensue to some extent. Thus we allow for the possibility of subsequent misalignment of the magnetic axis that, upon further cooling back below the deconfinement temperature, can trigger the same process as before to give subsequent bursts. One might expect these bursts strengths to depend on the amount of heating and resulting misalignment. Possible sources of subsequent heating can include accretion from a companion, impact from the accretion of a small body, or the quark star passing through a higher density region in the ISM. This leads to the prediction that radio emission should pick up again slightly before the subsequent bursts, provided there is a favourable line-of-sight. The accurate measurement of the temperature in the star in these subsequent bursts would now allow observations of the deconfinement temperature, which has eluded QCD physicists so far.

The quiescent phase is due to vortex expulsion from spin-down and subsequent annihilation through magnetic reconnection near the surface. The number of vortices decrease slowly with spin-down leading to continuous, quiescent energy release which can last for 10^3 to 10^4 years (see Ouyed et al. 2004 for more details).

4. Model predictions and observational tests

In the light of the results presented above we will now discuss our model predictions and offer our interpretation of the open issues listed in § 1.1:

- Following reorganization of the outer magnetic field and its alignment with the rotation axis, our model naturally predicts the suppression of further radio pulsations. Our model can thus in principle explain why SGRs and AXPs stop pulsating following their bursting era.
- The high- B (magnetar-strength) radio pulsars that show no evidence of enhanced X-ray emission, can be accounted for in our model if they are just neutron stars that have not experienced the Meissner effect. As long as the object is a quark star in a superconducting phase, magnetic field decay and reorganization will take effect regardless of the field strength. We thus predict that SGR-like bursts with moderate-strength magnetic field may be discovered in the future.
- If observations do confirm that the progenitors of SGRs are very massive stars (Gaensler et al. 2005) this would strengthen our model since massive progenitors are more likely to lead to massive neutron stars, for which it should be easier to reach deconfinement densities in the core following accretion or spin-down.
- The period clustering of observed SGRs and AXPs can be explained in our model as the time necessary for the parent neutron star to cool down sufficiently to experience a transition to a quark star.

Other predictions from our model are:

- The association of the SGR source (the quark star) with a parent radio-pulsar. In other words, in at least a few cases (if beaming is favorable) a parent radio-pulsar should be detected in the same location in the sky as the SGR before the bursting activity.
- If observations show quiescent emission before and after the burst then this is a subsequent burst in our picture, meaning the SGR will have been a quark star for some time. In this case the association with a parent neutron star will be less obvious.
- Assuming synchrotron dominated emission, we should observe a peak at ~ 280 keV ($B/5 \times 10^{13}$ G) for a solar mass quark star with a 10 km radius.
- The total energy in bursts from moderate-strength magnetic field (10^{12} G) quark stars would be much weaker according to Eq. 6. We predict burst energy from these stars to be of the order of 10^{40} erg.
- Finally, we note that during the stars phase transition from hadronic to quark matter, its radius changes from 30% - 50% (Ouyed et al. 2002), naturally resulting in a significant increase of the magnetic field at the surface. Therefore, a quark star with a strong magnetic field is not necessarily the result of a parent star with a strong magnetic field. So, if quark stars undergoing the Meissner effect are indeed the cause of SGRs or AXPs, then stronger field strengths in these objects should be expected.

5. Conclusion

We presented 3-D simulations of the reorganization of the magnetic field surrounding a newly born quark star. The reorganization is a consequence of the star entering the CFL phase, confining the interior field to vortices, and leaving the exterior field in its tilted dipole configuration. In our model the bursting activity in SGRs and AXPs is explained as magnetic reconnection events occurring while the exterior field aligns itself with the interior one. One of the obvious consequences of the final state (aligned rotator) is the suppression of the radio-emission in SGRs and AXPs following their bursting era. We should emphasize that magnetic fields alone cannot be responsible for the properties of SGRs and AXPs, but rather a compact star experiencing the Meissner effect is required. A further consequence is that while a low- B quark star entering the “Meissner phase” would burst in X-ray, this will not necessarily be the case for a high- B neutron star. While quark stars have not yet been observed in nature, our model seems to account for many observed features in SGRs and AXPs, thus warranting further investigation.

We thank Ralph Pudritz, Chris Pethick, and Kaya Mori for discussions. B. N. thanks C.I.T.A. for hospitality, and Sigma-Xi for its Grant-in-aid of research. The research of R. O. is supported

by grants from the Natural Science and Engineering Research Council of Canada (NSERC) and Alberta Ingenuity Fund (AIF).

A. Magnetic energy of a vertical field in a sphere

Consider a strictly vertical magnetic field $\vec{B} = B_z(x, y)\hat{z}$ in a sphere of radius R . Since the radial component of \vec{B} must be continuous at the surface, the field inside the sphere must be

$$B_z(r, \vartheta, \varphi) = \frac{B_r(R, \Theta, \varphi)}{\cos \Theta} , \quad (\text{A1})$$

where Θ is the colatitude at the surface, which is related to r, ϑ via

$$r \sin \vartheta = R \sin \Theta = s , \quad (\text{A2})$$

with s the cylindrical radius. To calculate the magnetic energy inside the sphere, we integrate \vec{B}^2 over z , then transform the s integral in one over Θ , using Eq. (A2). After a bit of algebra, we find the remarkable expression

$$E_{\text{mag}} = R^3 \int_0^{2\pi} d\varphi \int_0^\pi d\Theta \sin \Theta \frac{B_r^2(R, \Theta, \varphi)}{2\mu_0} . \quad (\text{A3})$$

B. Initial magnetic field configuration

The initial magnetic field represents the phase where the Meissner effect has forced the field inside the neutron star to be strictly vertical, but this reorganization has not yet had time to affect the external field.

In order to keep magnetic energy finite, we have to allow for a transition layer between the vertical internal field and the inclined dipolar external field. We are thus looking for a magnetic field configuration that minimizes total magnetic energy under the following requirements:

1. For $r > R_2$, the magnetic field is that of a dipole of dipole moment \vec{m} , inclined by ϑ_2 with respect to the vertical axis
2. For $r < R_1$, the field is strictly vertical.

Minimizing the magnetic energy in the transition layer $R_1 < r < R_2$ implies that \mathbf{B} is a potential field in that region.

To find the minimum energy field satisfying these requirements, we represent the magnetic field through scalar potentials S and T :

$$\vec{B} = -\nabla \times (\vec{x} \times \nabla S) - \vec{x} \times \nabla T . \quad (\text{B1})$$

Both the vertical field and the inclined dipole field do not have a toroidal part T , thus we set $T = 0$ everywhere. For the poloidal scalar potential S , we make the ansatz

$$S = \sum_{m=-1}^1 \left(a_1^m r + \frac{b_1^m}{r^2} \right) Y_1^m(\vartheta, \varphi) . () , \quad (\text{B2})$$

where $Y_1^m(\vartheta, \varphi)$ are the spherical harmonics of order 1 and degree m . Equation (B2) is compatible with both the inner and the outer field; any spherical harmonics of higher order would only increase the total energy, so we do not include them.

Minimizing the sum of the energy (A3) [with $R = R_1$] and the energy of the potential field for $R_1 < r < R_2$, we find the following coefficients for S after a straight-forward, but somewhat tedious calculation:

$$a_1^m = \tilde{a}_m \beta_1^m , \quad b_1^m = \tilde{b}_m \beta_1^m , \quad (\text{B3})$$

where

$$\beta_1^m = \frac{\mu_0 |\vec{m}|}{4\pi} \sqrt{\frac{4\pi}{3}} \begin{cases} \cos \vartheta_2 & , m = 0 \\ \mp \frac{\sin \vartheta_2}{\sqrt{2}} & , m = \pm 1 \end{cases} , \quad (\text{B4})$$

and

$$\tilde{a}_0 = \begin{cases} \frac{1}{R_2^3} & , r < R_1 \\ \frac{1}{R_2^3} & , R_1 < r < R_2 \\ 0 & , r > R_2 \end{cases} \quad (\text{B5})$$

$$\tilde{a}_{\pm 1} = \begin{cases} 0 & , r < R_1 \\ \frac{1}{R_2^3 - R_1^3} & , R_1 < r < R_2 \\ 0 & , r > R_2 \end{cases} \quad (\text{B6})$$

$$\tilde{b}_0 = \begin{cases} 0 & , r < R_1 \\ 0 & , R_1 < r < R_2 \\ 1 & , r > R_2 \end{cases} \quad (\text{B7})$$

$$\tilde{b}_{\pm 1} = \begin{cases} 0 & , r < R_1 \\ -\frac{R_1^3}{R_2^3 - R_1^3} & , R_1 < r < R_2 \\ 1 & , r > R_2 \end{cases} \quad (\text{B8})$$

To obtain the magnetic vector potential (which we need for the PENCIL CODE), we use the formula

$$\vec{A} = -\vec{x} \times \nabla S . \quad (\text{B9})$$

For a thin transition layer of thickness $\varepsilon \equiv R_2 - R_1 \ll R_1$, the contributions to the magnetic energy are

$$E(r > R_2) = E_2 \equiv \frac{\mu_0 \vec{m}^2}{12 \pi R_2^3}, \quad (B10)$$

$$E(r_1 < r < R_2) = \frac{\sin^2 \vartheta_2}{\varepsilon} E_2 + O(1), \quad (B11)$$

$$E(r > R_2) = 2 \cos^2 \vartheta_2 E_2 + O(\varepsilon). \quad (B12)$$

REFERENCES

Alcock, C., Farhi, E., & Olinto, A. 1986, ApJ, 310, 261

Alford, M. G., Rajagopal, K. & Wilczek, F., Phys. Lett. B 422 (1998), p. 247

Alford, M. G., Rajagopal, K. & Wilczek, F., Nucl. Phys. B 537 (1999), p. 443

Alford, M., Berges, J., & Rajagopal, K. 2000, Nucl. Phys. B, 571, 269

Alford, M., Bowers, J. A., & Rajagopal, K. 2001, Phys. Rev. D, 63, 074016

Alpar, M. A. 1991, in Neutron Stars, Theory and Observation (Ventura, J. & Pines, D.), Kluwer, Amsterdam, 1991, 49.

Arnold, P., Moore, G. D., & Yaffe, L. G. 2000, Journal of High Energy Physics, 11, 001

Bailin, D., & Love, A. 1984, Phys. Rep., 107, 325

Baring, M. G., & Harding, A. K. 2001, ApJ, 547, 929

Barrois, B. C. 1977, Nucl. Phys. B 129, 390.

Baym, G., & Heiselberg, H. 1997, Phys. Rev. D, 56, 5254

Blaschke, D., Grigorian, H., & Voskresensky, D. 2001, A&A, 368, 561

Bombaci, I., & Datta, B. 2000, ApJ, 530, L69

Carter, G. W., & Reddy, S. 2000, Phys. Rev. D, 62, 103002

Chatterjee, P., Hernquist, L., & Narayan, R. 2000, ApJ, 534, 373

Chevalier, R. N. 1989, ApJ, 346, 847

Cline, T. L. et al. 1980, ApJ, 237, L1

Coe, M. J., Jones, L. R., & Lehto, H. 1994, MNRAS, 270, 178

Collins, J. C. & Perry, M. J., Phys. Rev. Lett. 34 (1975), p. 1353.

Corbett, R. H. D., et al. 1995, ApJ, 443, 786

Dobler, W., Stix, M. & Brandenburg, A. 2006, ApJ, (accepted).

Duncan, R. C. & Thompson, C. 1992, ApJ, 392, L9

Fenimore, E. E., Klebesadel, R. W., & Laros, J. G. 1996, ApJ, 460, 964

Feroci, M., Hurley, K., Duncan, R. C., & Thompson, C. 2001, ApJ, 549, 1021

Fukue, J. 2001, PASJ, 53, 687

Gaensler, B. M., Slane, P. O., Gotthelf, E. V., & Vasisht, G. 2001, ApJ, 559, 963

Gaensler, B. M. 2002, astro-ph/0212086

Gaensler, B. M., McClure-Griffiths, N. M., Oey, M. S., Havercorn, M., Dickey, J. M., & Green, A. J. 2005, ApJ, 620, L95

Gavriil, F. P., Kaspi, V. M., & Woods, P. M. 2002, Nature, 419, 142

Glendenning, N. K. 1997, Compact stars (Springer)

Goldreich, P. & Reisenegger, A. 1992, ApJ, 395, 250

Golenetskij, S. V., Mazets, E. P., Ilinskij, V. N., & Guryan, Y. A. 1979, Soviet Astronomy Letters, 5, 340

Gonzalez, M., & Safi-Harb, S. 2003, ApJ, 591, L143

Gonzalez, M. et al. 2004, ApJ, 605, 368

Graham-Smith, F. 2003, Rep. Prog. Phys. 66, 173

Haensel, P. 1991, Nucl. Phys. B (Proc. Suppl.), 24, 23

Heger, A., Woosley, S. E., & Spruit, H. C. 2004, ApJ, submitted (astro-ph/0409422)

Heiselberg, H., & Pethick, C. J. 1993, Phys. Rev. D, 48, 2916

Horvath, J. E., Benvenuto, O. G., & Vucetich, H. 1991, Phys. Rev. D, 44, 3797

Hurley, K. et al. 1999a, Nature, 397, 41

Hurley, K. et al. 1999b, ApJ, 510, L111

Ibrahim, A. I. et al. 2001, ApJ, 558, 237

Iida, K. & Baym, G. 2002, PRD, 66, 14015

Iwamoto, N. 1980, Phys. Rev. Lett., 44, 1637

Iwamoto, N. 1982, Ann. Phys., 141, 1

Iwasawa, K., Koyama, K., & Halpern, J. P. 1992, PASJ, 44, 9

Kaplan, D. L., 2000, in Spin, Magnetism and Cooling of Young Neutron Stars,
http://online.itp.ucsb.edu/online/neustars_c00/

Kaplan, D. L. 2002, Memorie della Societa Astronomica Italiana, 73, 496

Kaspi, V. M. et al., 2003, Ap.J., 588, L93.

Kaspi, V. M., 2004, astro-ph/0402175

Kaspi, V. & McLaughlin, M. A. 2005, ApJ, 618, L41

Keränen, P., & Ouyed, R. 2003, A&A, 407, L51.

Keränen, P., Ouyed, R., & Jaikumar, P. 2005, ApJ, 618, 485

Kouveliotou, C. et al. 1998, Nature, 393, 235

Kouveliotou, C. et al. 1999, ApJ, 510, L115

Kriss, G. A. et al. 1985, ApJ, 288, 703

Kulkarni, S. R., Kaplan, D. L., Marshall, H. L., Frail, D. A., Murakami, T., & Yonetoku, D. 2003, ApJ, 585, 948

Lorimer, D. R., Lyne, A. G., & Camilo, F. 1998, A&A, 331, 1002

Manchester, R. N. & Taylor, J. H. 1977, San Francisco : W. H. Freeman, c1977., 36

Mazets, E. P., Golenetskii, S. V., Ilinskii, V. N., Aptekar, R. L., & Guryan, I. A. 1979, Nature, 282, 587

Mazets, E. P., Cline, T. L., Aptekar', R. L., Butterworth, P. S., Frederiks, D. D., Golenetskii, S. V., Il'inskii, V. N., & Pal'shin, V. D. 1999, Astronomy Letters, 25, 635

McLaughlin, M. A. et al. 2003, ApJ, 591, L135

Meissner, W., Ochsenfeld, R., 1933, Naturwiss., 21, 787

Mereghetti, S. 2000, in The Neutron Star-Black Hole Connection, ed. V. Connaughton, C. Kouveliotou, J. Van Paradijs & J. Ventura (NATO-ASI), in press (astro-ph/9911252)

Ouyed, R., Dey, J., & Dey, M. 2002, A&A, 390, L39

Ouyed, R., Elgarøy, Ø, Dahle, H., & Keränen, P. 2004, A&A, 420, 1025

Paczynski, B. 1992, Acta Astron., 42, 145

Page, D., & Usov, V. V. 2002, PRL, 89, 1311011

Pisarski, R. D. & Rischke, D. H., Phys. Rev. Lett. 83 (1999), p. 37

Pivovaroff, M., Kaspi, V., & Camilo, F. 2000, ApJ, 535, 379

Rapp, R., Schäfer, T., Shuryak, E. V., & Velkovsky, M., Phys. Rev. Lett. 81 (1998), p. 53

Rischke, D. H., 2000, Phys. Rev. D 62, 034007

Rischke, D. H., 2000, Phys. Rev. D 62, 054017

Ruutu, V. M., Ruohio, J. J., Krusius, M., Plaçais, B., Sonin, E. B., & Xu, W. 1997, PRB, 56, 14089

Rybicki, G. B., & Lightman, A. P. in Radiative Processes in Astrophysics, 1979 (Wiley & Sons).

Schäfer, T., (hep-ph/0304281).

Sedrakian, D. M., Blaschke, D., Shahabasyan, K. M., & Voskresensky, D. N. 2001, Astrofizika, 44, 443

Shovkovy, I. A., & Ellis, P. J. 2003, Phys. Rev. C, 67, 048801

Son, D. T., Phys. Rev. D 59 (1999), p. 094019

Thompson, C. & Duncan, R. C. 1995, MNRAS, 275, 255

Thompson, C. & Duncan, R. C. 1996, ApJ, 473, 322

Tilley, D. R., & Tilley, J. Superfluidity and Superconductivity, 3rd ed., Bristol, England, Hilger 1990

Tsubota, M., Kasamatsu, K., & Ueda, M. 2002, Phys. Rev. D, 65, 023603

Usov, V. V. 2001, Physical Review Letters, 87, 021101

van Kerkwijk, M. H., & Kulkarni, S. R. 2001, A&A, 380, 221

Vancura, O., Blair, W. P., Long, K. S., & Raymond, J. C. 1992, ApJ, 394, 158

Woods, P. M. et al. 1999, ApJ, 527, L47

Woods, P. M., Kouveliotou, C., Göğüş, E., Finger, M. H., Swank, J., Markwardt, C. B., Hurley, K., & van der Klis, M. 2002, ApJ, 576, 381

Woods, P. M., 2003, astro-ph/0304372

Woods, P. M. et al., 2003, astro-ph/0310575

Zane, S., Turolla, R., Stella, L., & Treves, A. 2001, ApJ, 560, 384

Zhang, B., & Harding, A. K. 2000, ApJ, 535, L51

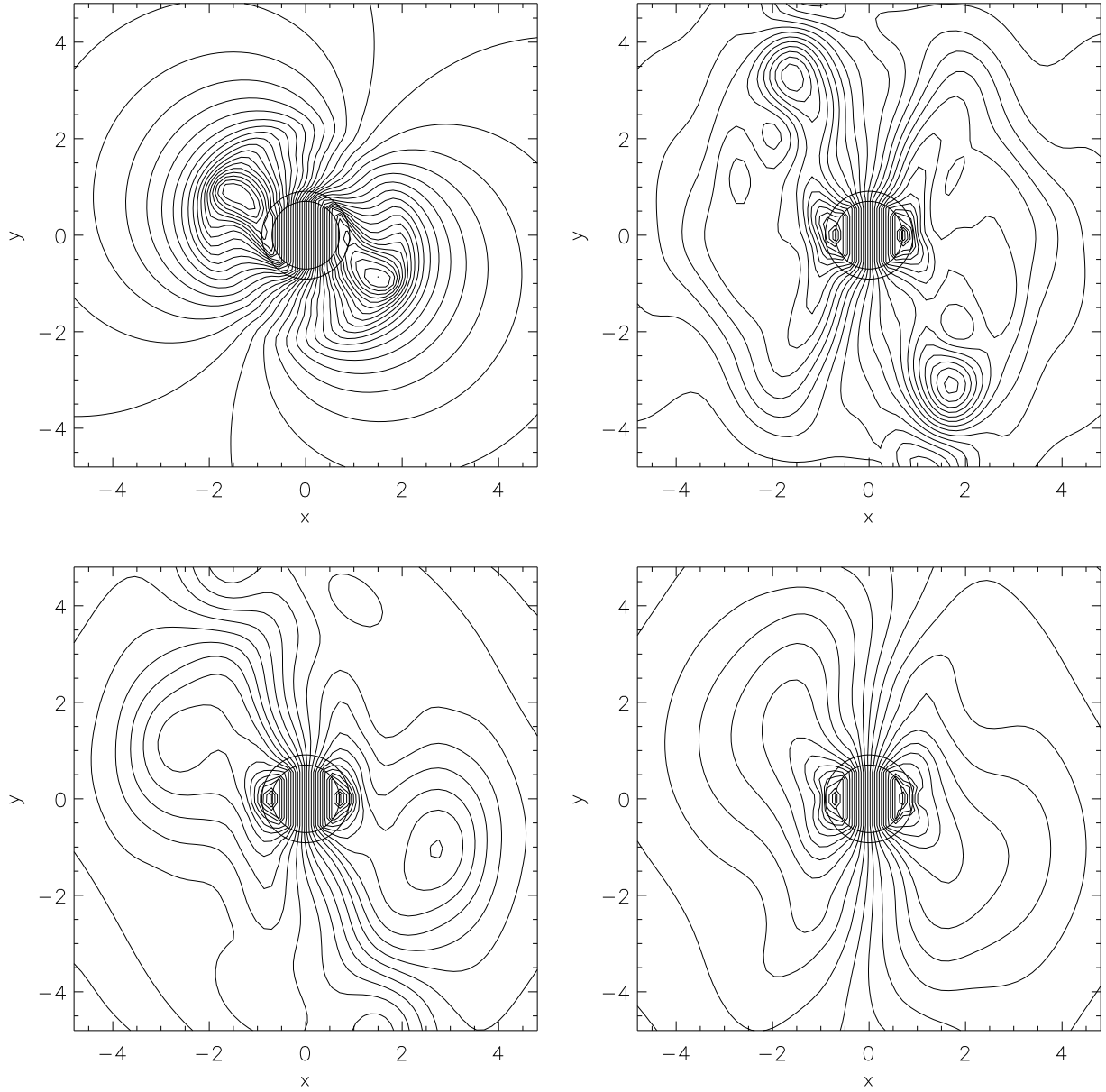


Fig. 2.— “Mock magnetic field lines” in the xz -plane (rotation axis is along z) at $t = 1, 25, 100, 300$ going left to right, top to bottom. Note the Alfvén front at $t = 1$, which is accompanied by reconnection events. Reconnection events become more apparent with time as the surface magnetic field re-adjusts itself. In the last frame we see an aligned dipole which would mark the end of radio activity.

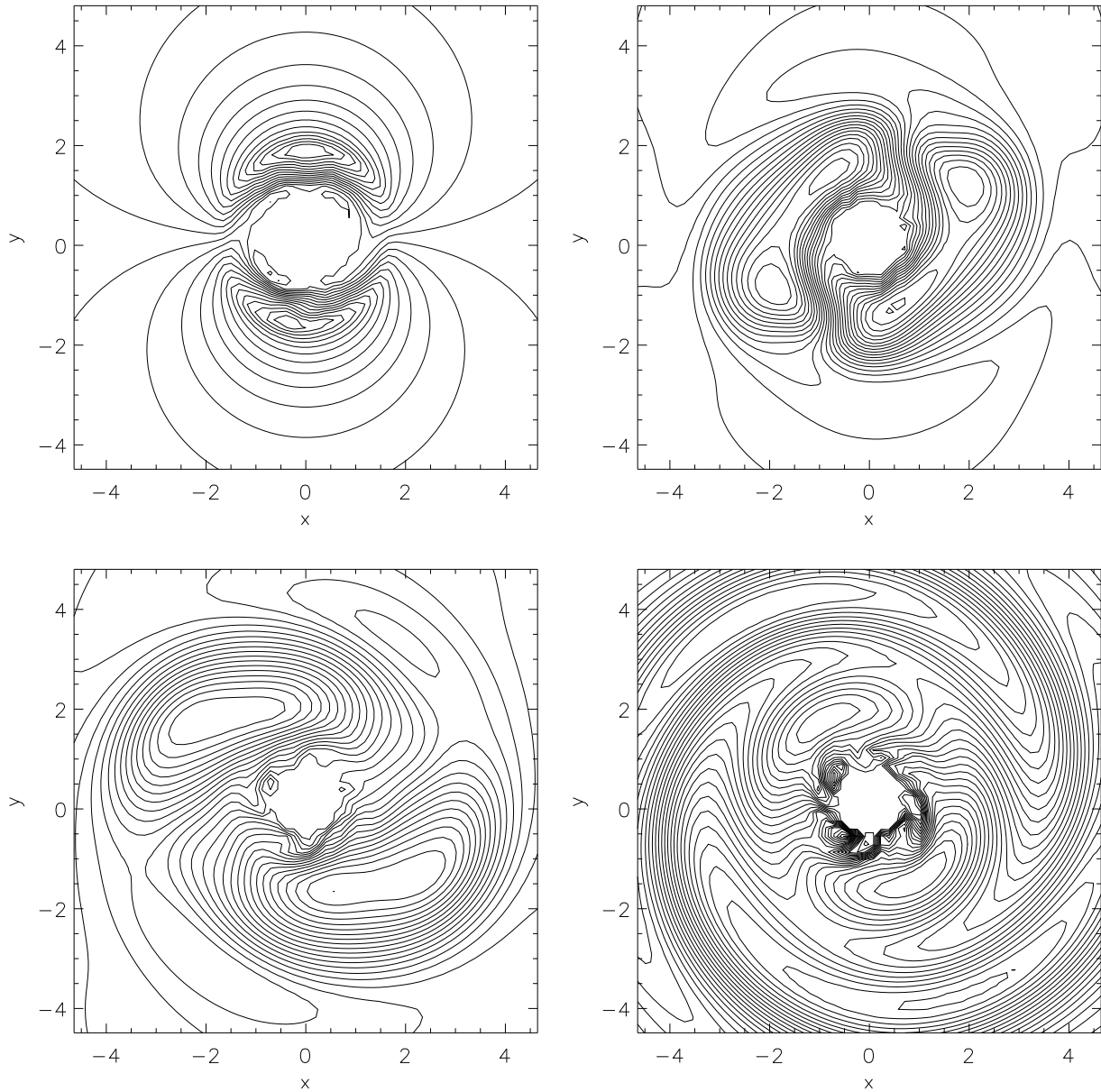


Fig. 3.— “Mock magnetic field lines” in the xy -plane (down the rotation axis) at $t = 1, 25, 100, 300$ going left to right, top to bottom.

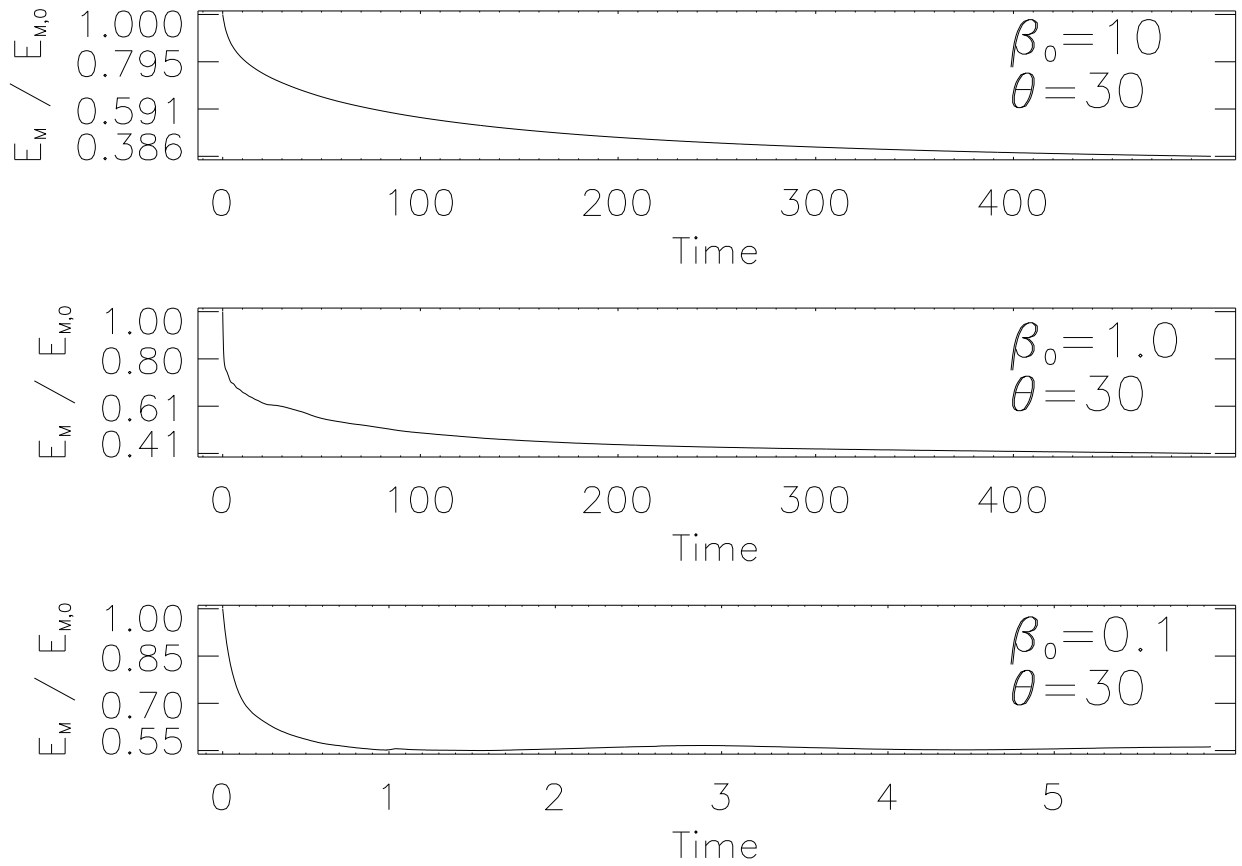


Fig. 4.— Magnetic energy lost over time. The change in magnetic energy (α in Eq. 6) can be estimated from these plots to be between 0.4 – 0.6, implying that energies of order 10^{44} erg are released during the event.

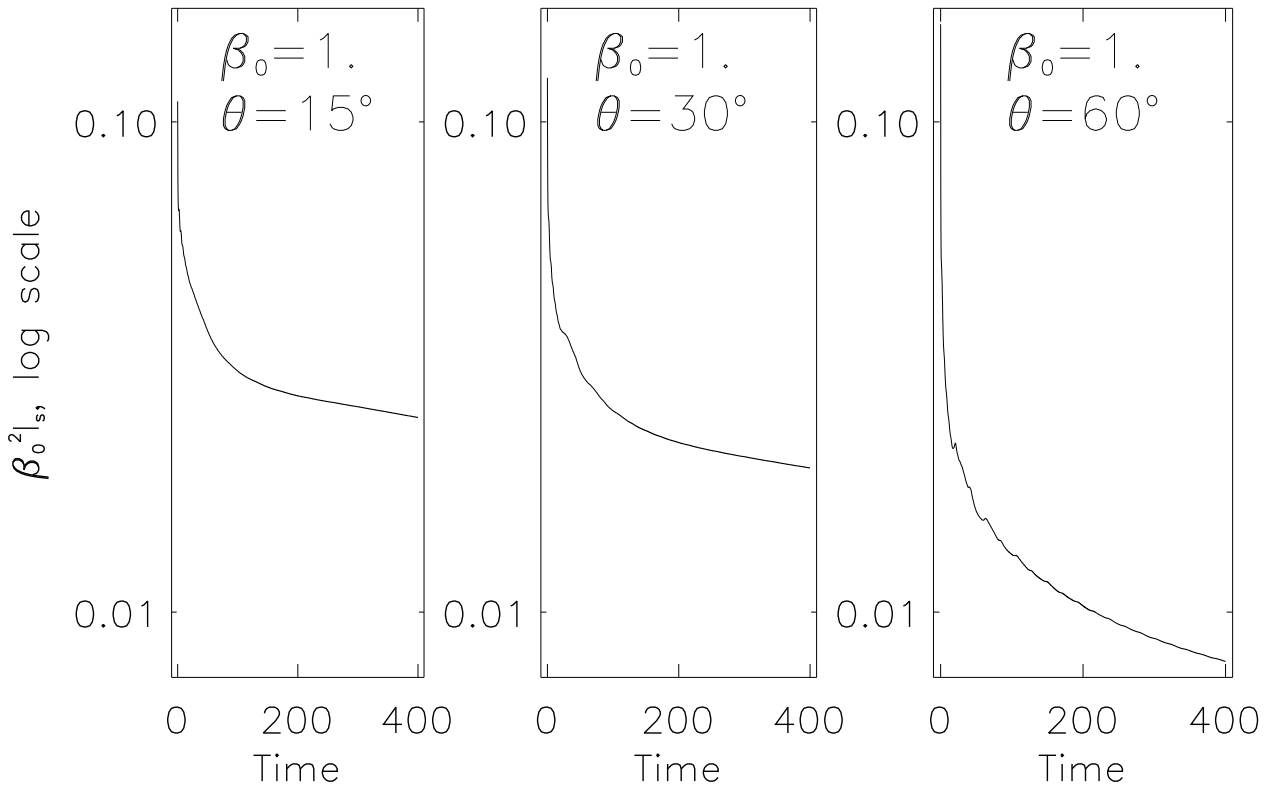


Fig. 5.— Total intensity emitted ($\beta_0^2 I_s$) versus time for $\beta = 0.3$ and $\theta = 15^\circ, 30^\circ, 60^\circ$ (angle between rotation and initial magnetic dipole axis). We note that the higher the inclination angle, the longer it takes for the outer magnetic field to align itself. This can be seen in the figures where the tail takes longer to flatten for higher angles. Furthermore, the high inclination run shows oscillations which can be linked to stronger reconnection events.

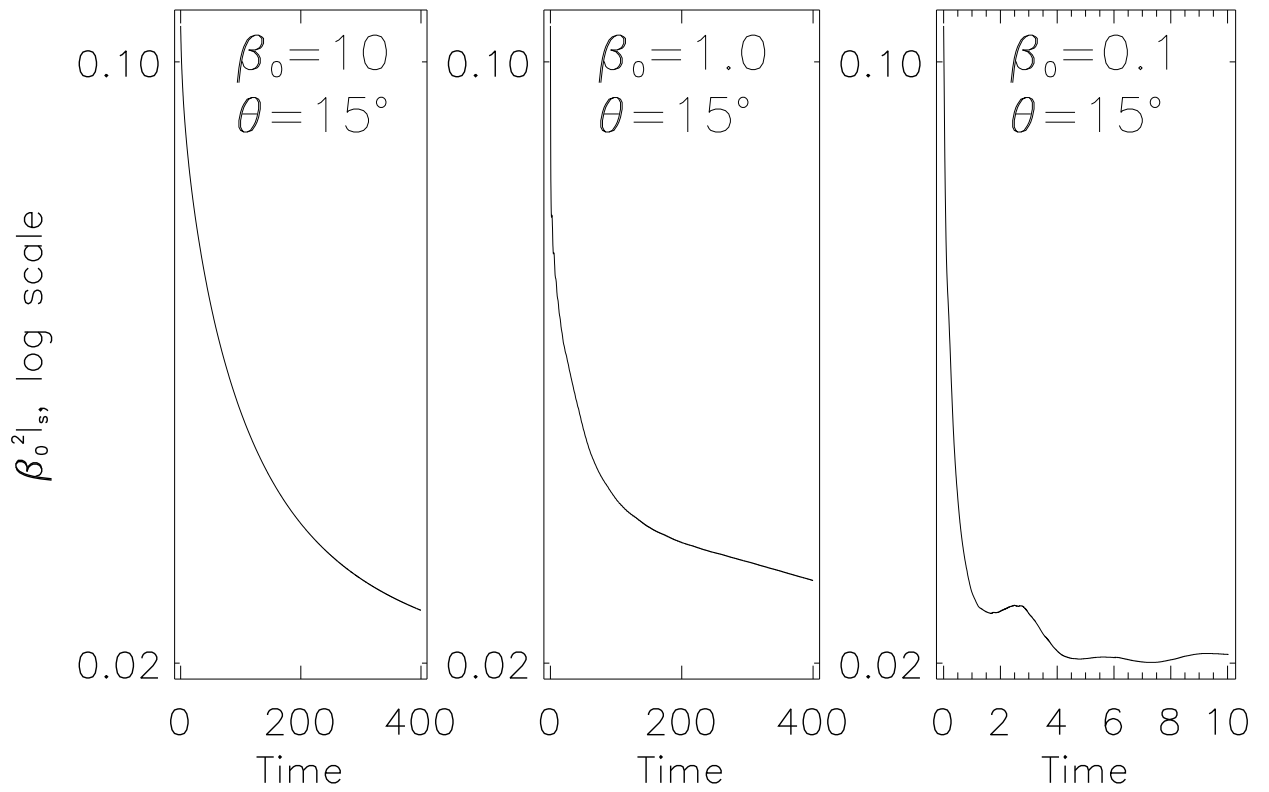


Fig. 6.— Total intensity emitted ($\beta_0^2 I_s$) versus time for $\theta = 15^\circ$ and $\beta = 10, 1, 0.1$. We note that the higher β , the slower the re-adjustment and flattening of the tail. The decrease in variability with increasing β can be explained by a decrease in amplitude of magnetic “breathing” modes.

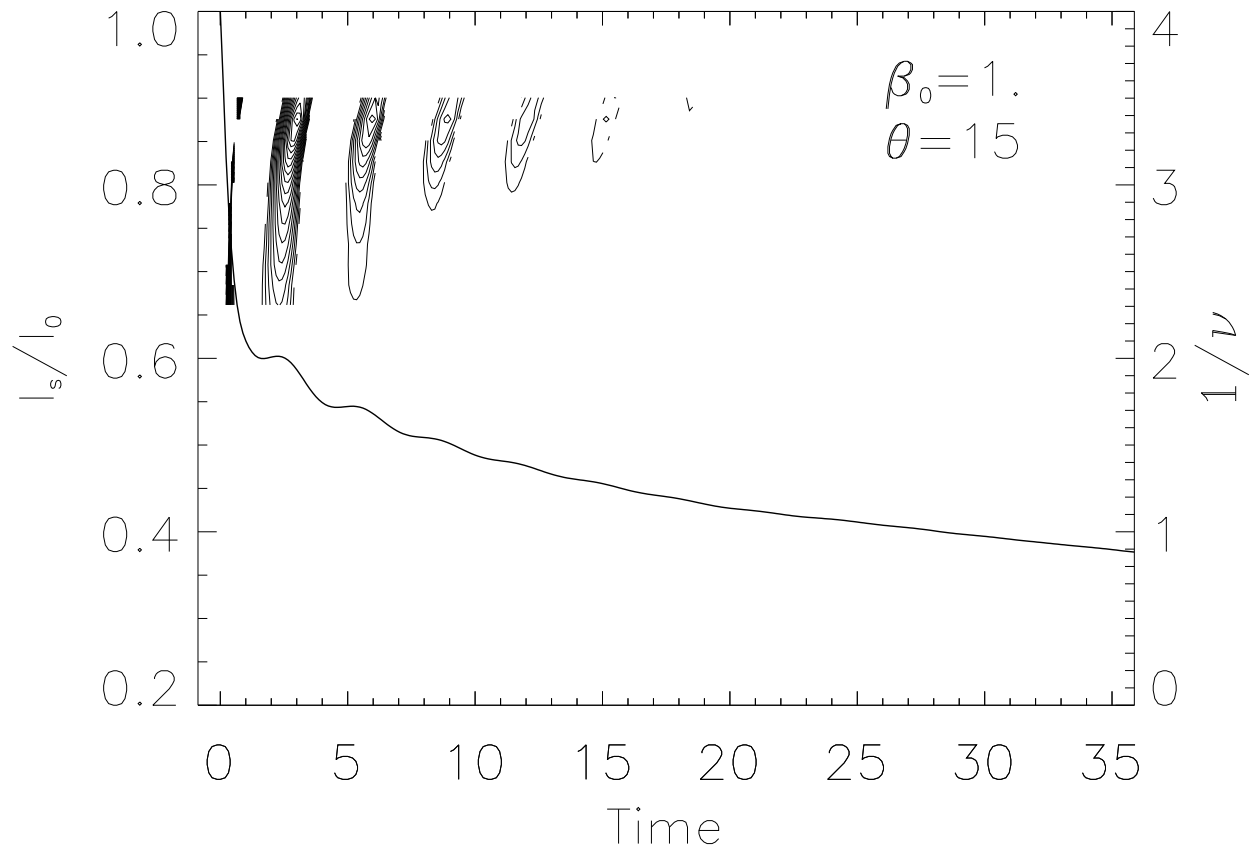


Fig. 7.— Time evolution of the Fourier-power spectrum (contours, right axis) for $\beta = 1$ and $\theta = 15^\circ$ along with the normalized intensity (solid line, left axis). The sub-pulses in intensity are shown here to be modulated at ~ 3.25 times the spin-period. In an observer's frame, this modulation should be further modulated by the spin period.

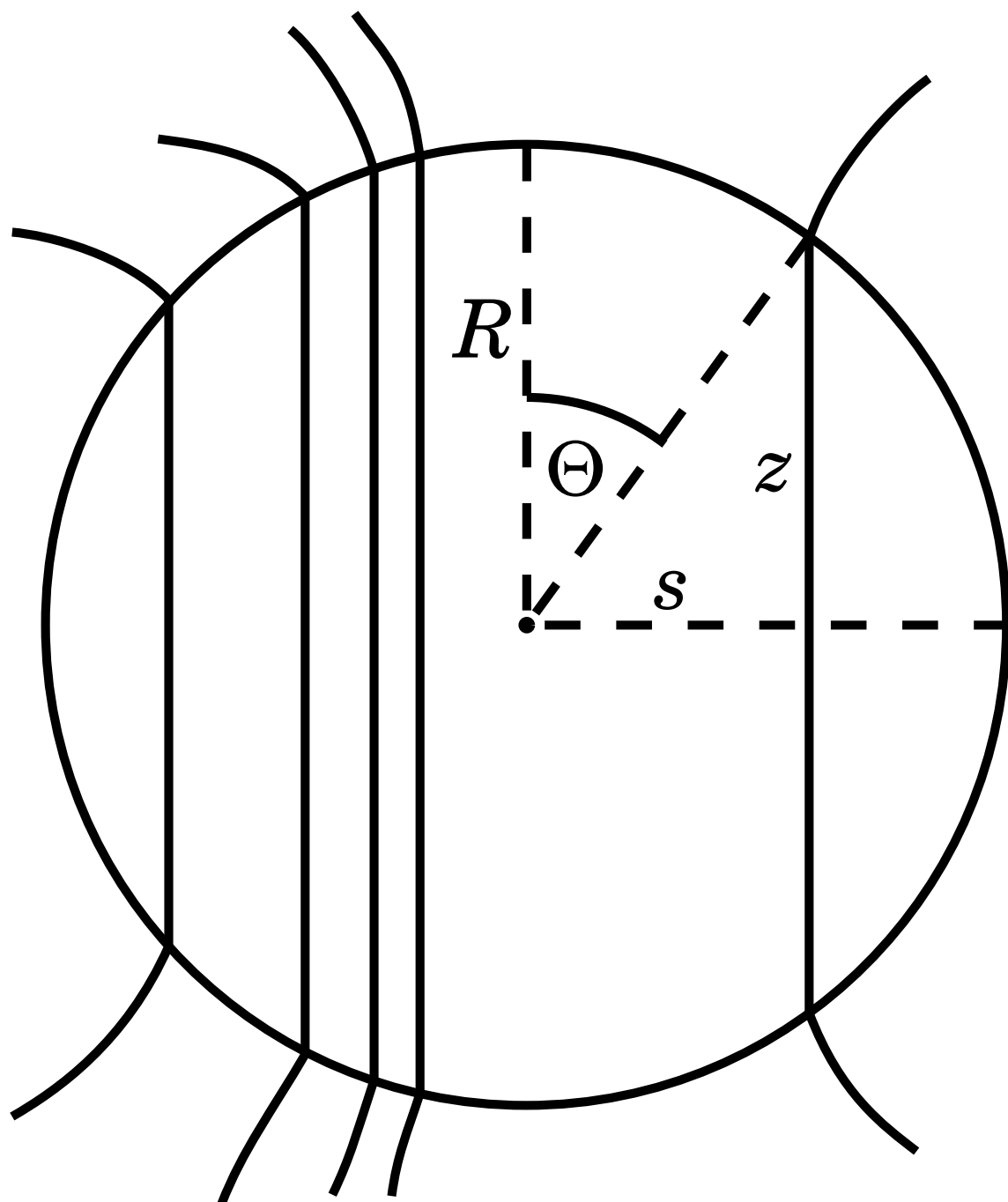


Fig. 8.— Sketch of magnetic field inside and outside the sphere.